Available online at www.sciencedirect.com
SCIENCE DIRECT®
Journal of Computational Physics 208 (2005) 34–50
JOURNAL OF COMPUTATIONAL PHYSICS
www.elsevier.com/locate/jcp

An iterative-perturbation scheme for treating inhomogeneous elasticity in phase-field models

P. Yu [a], S.Y. Hu [b], L.Q. Chen [b], Q. Du [a,b,*]

[a] *Department of Mathematics, Penn State University, State College, PA 16802, United States*
[b] *Department of Materials Science and Engineering, Penn State University, State College, PA 16802, United States*

Received 22 July 2004; received in revised form 10 January 2005; accepted 1 February 2005
Available online 25 April 2005

Abstract

In this paper, we discuss a simple iterative-perturbation scheme for solving the elasticity equation in systems with strong elastic inhomogeneity. As an example, a thin film in contact with a gas and a substrate is considered. The scheme is demonstrated to be efficient through numerical experiments and reliable through rigorous mathematical justification. It is then applied to the study of the inhomogeneous shear modulus effect on the microstructure evolution in thin films based on the phase-field method.

Keywords: Inhomogeneous elasticity; Phase-field; Thin film; Microstructure evolution; Iterative scheme; Fourier-spectral

1. Introduction

The phase-field method has recently emerged as a powerful computational approach to model and predict the mesoscale morphological and microstructure evolution in materials. Unlike conventional methods which model the regions separating the compositional or structural domains as sharp interfaces, the phase-field approach is based on a diffuse-interface description using a set of conserved and non-conserved field variables that are continuous across the interfacial regions. The temporal and spatial evolution of the phase variables is governed by the Cahn–Hilliard diffusion equation and the Allen–Cahn relaxation equation. With the fundamental thermodynamic and kinetic information as the input, the phase-field method is able to predict the evolution of arbitrary morphologies and complex microstructures without explicitly tracking the positions of interfaces. We refer the readers to [1] for a review of the recent advances in developing

* Corresponding author. Tel.: +1 814 865 3674; fax: +1 814 865 3735.
E-mail address: qud2@psu.edu (Q. Du).

0021-9991/$ - see front matter © 2005 Elsevier Inc. All rights reserved.
doi:10.1016/j.jcp.2005.02.015

phase-field models for various materials processes including solidification, solid-state structural phase transformations, grain growth and coarsening, domain evolution in thin films, pattern formation on surfaces, dislocation microstructures, crack propagation, and electro-migration.

Microstructure evolution takes place to reduce the total free energy that may include the bulk chemical free energy, interface energy, and long-range interaction energies such as elastic energy and electrostatic energy. Suppose that the two types of field variables, conserved and non-conserved, are denoted by $(c_1, c_2, \ldots, c_n)$ and $(\eta_1, \eta_2, \ldots, \eta_p)$. The total free energy of an inhomogeneous microstructure system described by these field variables is then given by

$$F = \int \left[f(c_1, c_2, \ldots, c_n, \eta_1, \eta_2, \ldots, \eta_p) + \sum_{i=1}^{n} \alpha_i (\nabla c_i)^2 + \sum_{i=1}^{3} \sum_{j=1}^{3} \sum_{k=1}^{p} \beta_{ij} \nabla_i \eta_k \nabla_j \eta_k \right] \mathrm{d}^3 x + \int \int G(\boldsymbol{x} - \boldsymbol{x}') \, \mathrm{d}^3 x \, \mathrm{d}^3 x',$$

where f is the local free energy density, α_i and β_{ij} are the gradient energy coefficients. The first volume integral represents the local contribution to the free energy from short-range chemical interactions. The origin of interfacial energy comes from the gradient energy terms that are non-zero only at and around the interfaces. The second volume integral represents a non-local term that contains contributions to the total free energy from any one or more of the long-range interactions, such as elastic interactions, electric dipole–dipole interactions, electrostatic interactions, etc. The main differences among different phase-field models lie in the treatment of various contributions to the total free energy. With a given total free energy F, the evolution of the field variables can be obtained by solving the Cahn–Hilliard and Allen–Cahn equations,

$$\frac{\partial c_i(\boldsymbol{x}, t)}{\partial t} = \nabla \cdot M_{ij} \nabla \frac{\delta F}{\delta c_j(\boldsymbol{x}, t)},$$

$$\frac{\partial \eta_k(\boldsymbol{x}, t)}{\partial t} = -L_{kl} \frac{\delta F}{\delta \eta_l(\boldsymbol{x}, t)},$$

where the kinetic coefficients M_{ij} and L_{kl} are related to atom or interface mobility, and the operator δ denotes the variation of the energy functional with respect to the field variables. In the above equations and throughout this paper, we use the summation convention that the same index appearing twice indicates summation over the range of the index. The summation sign "$\sum$" is used explicitly only when the index for summation does not appear in pairs.

Phase transformations in solids usually produce coherent microstructures at their early stages. In a coherent microstructure, the lattice planes and directions are continuous across the interfaces, and the lattice mismatch between phases and domains are accommodated by elastic displacements. The elastic energy contribution to the total free energy in a phase-field model can be introduced by expressing the elastic strain energy as a function of field variables, and the elastic energy is often a key thermodynamic and kinetic factor governing the temporal evolution of microstructures. Therefore, an efficient and accurate method to calculate the elastic energy is desirable for predicting microstructure evolution.

In an elastically homogeneous bulk solid with an arbitrary microstructure, Khachaturyan's microelasticity theory [2] provides an efficient approach to calculate the elastic energy. It has been applied to study the effect of elastic energy on microstructure evolution during various structural phase transformations [1]. For systems with weak elastic inhomogeneity, first-order approximations have been employed to solve the mechanical equations [3–5]. However, the numerical solution to the mechanical equilibrium equation becomes significantly more complicated for microstructures with strong elastic inhomogeneity. Recently, a number of approaches have been proposed, including the iterative-perturbation method [6], the preconditioned conjugate gradient method combined with the Fourier-spectral approximation to the differential

operators [7,8], the finite element method [9] and the method based on Eshelby's equivalent inclusion theory [10–13]. Among these, the iterative-perturbation method and conjugate gradient method are aimed at solving the mechanical equilibrium equation directly. On the other hand, the method based on the Eshelby's inclusion theory requires the solution of the following gradient flow equation:

$$\frac{\partial \varepsilon_{ij}^0(\boldsymbol{x},t)}{\partial t} = -L_{ijkl}\frac{\partial E^{inhom}}{\delta \varepsilon_{kl}^0(\boldsymbol{x},t)},$$

where E^{inhom} is the strain energy of the inhomogeneous system, and the solution $\varepsilon_{ij}^0(\boldsymbol{x})$ is the eigenstrain with which the elastically homogeneous system would be equivalent to the original inhomogeneous system.

The purpose of this article is twofold. First, we adapt the iterative-perturbation method proposed in [6] to solid–gas systems where the elastic inhomogeneity is at its maximum. Second, we provide a rigorous justification of our formulation of the inhomogeneous system and the iterative-perturbation algorithm. Our novel inclusion of the gas phase in the elastic system is inspired by the idea of diffuse-interface modeling popularized in the phase-field methodology. Instead of solving the elastic equations only in the solid phase while imposing stress-free boundary conditions at the sharp interface between the solid and gas phases, we treat the gas phase as an integral part of the system with zero elasticity modulus and create a diffuse interface over which the elasticity constants of the solid smoothly transit to zero in the gas. From this perspective, our approach can be viewed as an extension of the phase-field idea to the elasticity equations, and the advantages of the phase-field method over other sharp-interface approaches are automatically inherited by our approach. In particular, there is no need to track the geometry of the interface directly, and the system can most of the time be set up in a square (2D) or cubic (3D) domain where highly efficient spectral methods are applicable. In particular, we use the Fourier-spectral method in this paper to solve the elasticity equations with periodic boundary conditions. The use of periodic boundary conditions is very common in phase-field simulations of microstructure evolution [1]. The underlying philosophy is that we are modeling merely a small local sample of a large material specimen and periodic boundaries are applied to minimize the finite-size effect.

The inclusion of the gas phase with degenerate elasticity modulus in the elastic system may seem somewhat artificial, and causes natural concerns over the well-posedness of the elasticity system and the validity of the iterative-perturbation scheme. For example, the creation of a diffuse interface between the solid and gas phases may be thought of as a source of severe modeling and computational errors. Nevertheless, our numerical experiences [14] seem to give strong support to the efficiency of the iterative-perturbation and its convergence to physically reasonable solutions, so long as the diffuse interfaces are fairly resolved by the computational grid (which means in practice putting around 8 grid points across the gradient direction of the diffuse interface). Yet, this method has not been analyzed theoretically in our earlier work. In this paper, we intend to further justify this method with rigorous mathematical analysis and benchmark numerical tests. The analysis focuses on (1) the well-posedness of the elasticity system with possibly degenerate elasticity modulus; (2) the sharp interface limit of our diffuse-interface formulation of the elasticity system; and (3) the convergence of the iterative-perturbation scheme. The numerical examples are selected to illustrate the efficiency and convergence of the iterative-perturbation scheme.

Although we focus mostly on elastic equations alone in this paper, we present at the end of the paper a kinetic simulation coupling the elasticity field with the Cahn–Hilliard equation to study the effect of elastic inhomogeneity on the morphological pattern formation in thin films. Thin film problems are among the various applications that the iterative-perturbation approach is most suitable for. Upon introducing a gas phase in our formulation of the elasticity system, we may apply the iterative-perturbation scheme with the simple yet efficient Fourier-spectral method, without worrying about the stress-free boundary conditions at the film surface even when the film surface is curvy. On the other hand, without the gas phase, the stress-free boundary conditions at the film surface further complicate the application of Fourier-spectral methods. In the case of curvy film surfaces, alternative approaches such as sophisticated finite element

meshing schemes and adaptive techniques may be required. In the past, very few analytical solution procedures or efficient numerical methods were available for the elasticity problem in thin films. For example, in a monolayer subject to the substrate constrain, Lu and Suo [15] derived an elastic solution using the Green functions where the stresses in the thin film were assumed to be independent of the thickness. For a thick film with a spatial distribution of eigenstrains, Li et al. [16] developed an efficient method to calculate the elastic field assuming elastic homogeneity. Although their method can be extended to the case that the film and substrate have different elastic constants, it cannot handle problems with the elastic inhomogeneity associated with compositional and structural inhomogeneity in films. The efficiency of finite element methods also remains to be demonstrated when the problems involve moving interfaces. On the contrary, the iterative-perturbation approach to be described later provides a very simple and elegant solution procedure to elasticity equations in thin films and can be easily extended to deal with evolving film surfaces [17].

The paper is organized as follows. In Section 2, we discuss the mechanical equilibrium equations used in the phase-field description of the solid and gas systems. The iterative-perturbation scheme is then presented in Section 3. In Section 4, we discuss the formulation of such a scheme for the elastic solution in films with stress-free surfaces and substrate constraints. Some rigorous mathematical analysis is provided in Section 5. In Section 6, we present several numerical examples, and we conclude in Section 7.

2. Elasticity system and mechanical equilibrium equations

We give a general description of a system consisting of a solid phase and a gas phase. The gas phase represents voids or cracks where elastic constants are modeled as zero. We assume that the solid phase is a binary solid solution with a compositional inhomogeneity $c = c(\boldsymbol{x})$ which represents the mole fraction of solutes at the position $\boldsymbol{x}$, and the local elastic modulus tensor is a linear function of the compositional inhomogeneity. Therefore, the local elastic modulus tensor can be written as

$$\lambda_{ijkl}(\boldsymbol{x}) = \lambda^0_{ijkl} + \lambda'_{ijkl}\delta c(\boldsymbol{x}) \quad \text{in the solid phase,}$$

$$\lambda_{ijkl}(\boldsymbol{x}) = 0.0 \quad \text{in the gas phase,}$$

where $\delta c(\boldsymbol{x}) = c(\boldsymbol{x}) - c_0$, λ^0_{ijkl} is an elastic modulus tensor for the homogeneous solid solution with the composition c_0, and λ'_{ijkl} is a constant tensor representing the elastic inhomogeneity within the binary solid solution. We assume $\delta c(\boldsymbol{x})$ is constructed in such a way that the elastic modulus tensor experiences a smooth transition to degeneracy over a thin interface between the solid and gas phases. In addition, we assume that the local stress-free strain tensor can be described in terms of the compositional inhomogeneity $\varepsilon^c_{ij}(\boldsymbol{x})$. If the variation of the stress-free lattice parameter a with respect to the composition obeys the Vegard's law, the local stress-free strain associated with the compositional inhomogeneity is given by

$$\varepsilon^c_{ij}(\boldsymbol{x}) = \varepsilon_0 \delta c(\boldsymbol{x}) \delta_{ij},$$

where $\varepsilon_0 = \frac{1}{a}\frac{\mathrm{d}a}{\mathrm{d}c}$ is the composition expansion coefficient of the lattice parameter and δ_{ij} is the Kronecker-Delta function. Most crystal defects such as dislocations, grain boundaries and cracks can be described by their corresponding spatially dependent stress-free strain $\varepsilon^{\mathrm{def}}_{ij}(\boldsymbol{x})$ [18–24]. Therefore, the total stress-free strain tensor $\varepsilon^0_{ij}(\boldsymbol{x})$ associated with the compositional inhomogeneity and distributed defects is given by

$$\varepsilon^0_{ij}(\boldsymbol{x}) = \varepsilon^c_{ij}(\boldsymbol{x}) + \varepsilon^{\mathrm{def}}_{ij}(\boldsymbol{x}).$$

Let us use $\varepsilon_{ij}(\boldsymbol{x})$ to denote the total strain measured with respect to a reference lattice and assume linear elasticity. The Hooke's law gives the local elastic stress,

$$\sigma_{ij}^{\mathrm{el}} = [\lambda_{ijkl}^{0} + \lambda'_{ijkl}\delta c(\boldsymbol{x})][\varepsilon_{kl}(\boldsymbol{x}) - \varepsilon_{kl}^{0}(\boldsymbol{x})]. \tag{2.1}$$

During the evolution of microstructure, since the mechanical equilibrium with respect to elastic displacements is usually established much faster than any other physical processes, for any given composition distribution, the system is always at a mechanical equilibrium,

$$\frac{\partial \sigma_{ij}^{\mathrm{el}}}{\partial x_j} = 0, \tag{2.2}$$

where x_j is the jth component of the position vector $\boldsymbol{x}$. The total strain $\varepsilon_{ij}(\boldsymbol{x})$ may be represented as the sum of homogeneous and heterogeneous strains:

$$\varepsilon_{ij}(\boldsymbol{x}) = \bar{\varepsilon}_{ij} + \delta\varepsilon_{ij}(\boldsymbol{x}), \tag{2.3}$$

where the homogeneous strain $\bar{\varepsilon}_{ij}$ is defined such that

$$\int_v \delta\varepsilon_{ij}(\boldsymbol{x})\,\mathrm{d}^3x = 0.$$

The homogeneous strain is the uniform macroscopic strain characterizing the macroscopic shape and volume change associated with the total strain $\varepsilon_{ij}(\boldsymbol{x})$. Let us use $u_i(\boldsymbol{x})$ to denote the ith displacement component of the heterogeneous deformation. According to the strain and displacement relationship, the heterogeneous strain can be expressed as

$$\delta\varepsilon_{kl}(\boldsymbol{x}) = \frac{1}{2}\left[\frac{\partial u_k(\boldsymbol{x})}{\partial x_l} + \frac{\partial u_l(\boldsymbol{x})}{\partial x_k}\right]. \tag{2.4}$$

Substituting Eqs. (2.1), (2.3) and (2.4) to the mechanical equilibrium equation (2.2), one has

$$\left[\lambda_{ijkl}^{0}\frac{\partial^2}{\partial x_j \partial x_l} + \lambda'_{ijkl}\frac{\partial}{\partial x_j}\left(\delta c(\boldsymbol{x})\frac{\partial}{\partial x_l}\right)\right]u_k(\boldsymbol{x}) = \frac{\partial}{\partial x_j}[\lambda_{ijkl}^{0} + \lambda'_{ijkl}\delta c(\boldsymbol{x})][\varepsilon_{kl}^{0}(\boldsymbol{x}) - \bar{\varepsilon}_{kl}]. \tag{2.5}$$

Therefore, the determination of the equilibrium elastic field for an elastically inhomogeneous solid is reduced to solving the mechanical equilibrium equations (elasticity equations) (2.5) subject to appropriate boundary conditions, and in particular, periodic boundary conditions in this paper. Please notice that in the gas phase, both the left-hand and the right-hand sides of (2.5) are zero, and thus the uniqueness of the solution to (2.5) cannot be expected to hold in the gas phase. The appropriate sense for discussing the uniqueness of the solution will be spelled out later in our analysis.

3. Iterative-perturbation scheme

The key idea of the iterative-perturbation scheme is to split the inhomogeneous part of the elastic modulus tensor to the right-hand side of (2.5), thus transforming the inhomogeneous (possibly degenerate) elasticity problem to iterations of homogeneous (non-degenerate) systems. The nth iteration of the scheme reads

$$\lambda_{ijkl}^{0}\frac{\partial^2 u_k^n(\boldsymbol{x})}{\partial x_j \partial x_l} = \frac{\partial}{\partial x_j}[\lambda_{ijkl}^{0} + \lambda'_{ijkl}\delta c(\boldsymbol{x})][\varepsilon_{kl}^{0}(\boldsymbol{x}) - \bar{\varepsilon}_{kl}] - \lambda'_{ijkl}\frac{\partial}{\partial x_j}\left[\delta c(\boldsymbol{x})\frac{\partial u_k^{n-1}(\boldsymbol{x})}{\partial x_l}\right]. \tag{3.1}$$

Mathematically, the interesting change caused by this splitting is that the possible degeneracy of (2.5) (and the non-uniqueness of the solution in the gas phase) is hidden in the initial and boundary conditions for (3.1). Thanks to the constant coefficients on the left-hand side of (3.1), this equation can be solved by

the Fourier-spectral method. For instance, if one sets the inhomogeneous elasticity λ'_{ijkl} to 0, the zeroth-order approximation to (3.1) becomes

$$\lambda^0_{ijkl}\frac{\partial^2 u^0_k(\boldsymbol{x})}{\partial x_j \partial x_l} = \lambda^0_{ijkl}\frac{\partial \varepsilon^0_{kl}(\boldsymbol{x})}{\partial x_j},$$

where $u^0_k(\boldsymbol{x})$ denotes the kth component of the displacement. Solving this in the Fourier space [1], we have

$$v^0_k(\boldsymbol{g}) = -\mathrm{i}G_{ik}(\boldsymbol{g})g_j\lambda^0_{ijmn}\xi^0_{mn}(\boldsymbol{g}),$$

where $v^0_k(\boldsymbol{g})$ and $\xi^0_{mn}(\boldsymbol{g})$ are the Fourier transforms of $u^0_k(\boldsymbol{x})$ and $\varepsilon^0_{mn}(\boldsymbol{x})$, respectively, $\mathbf{g}$ is a reciprocal lattice vector, g_j is the jth component of $\mathbf{g}$, and $G_{ik}(\boldsymbol{g})$ is the inverse tensor to $(G^{-1}(\boldsymbol{g}))_{ik} = g^2\lambda^0_{ijkl}n_j n_l$ with $\boldsymbol{n} = \frac{\boldsymbol{g}}{|\boldsymbol{g}|}$. The inverse Fourier transform of $v^0_k(g)$ gives the real-space solution for the displacement field in the zeroth order approximation,

$$u^0_k(\boldsymbol{x}) = \frac{1}{(2\pi)^3}\int v^0_k(\boldsymbol{g})\mathrm{e}^{\mathrm{i}\boldsymbol{g}\cdot\boldsymbol{x}}\,\mathrm{d}^3\boldsymbol{g}.$$

For static problems, one may choose this as the initial iterate of the iterative-perturbation scheme. For kinetic problems, it is usually more efficient to take as the initial iterate the converged solution to the elasticity equations from the previous time step.

Numerically, the Fourier-spectral method can be implemented via the Fast Fourier Transform (FFT). For simplicity of counting operations, suppose that we discretize the elasticity system by N grid points along each of the three dimensions. The total computational cost of each step of the iterative-perturbation scheme via FFT is $\mathrm{O}(N^3\log^3 N)$. Typical iterative methods to solve the discretized (by finite-difference or finite-element for example) elasticity equations have computational costs in the order of kN^3, where the constant k depends on the sparseness of the coefficient matrix of the linear system. The higher accuracy one requires for the approximation of the differential operators, the less sparse a discretized system results, and the bigger the constant k becomes. In practice, in terms of the cost per iteration, our iterative-perturbation approach is competitive with other iteration methods for linear systems, while offering straightforward implementation and highly accurate approximations to the differential system. Of course, another key factor that affects the total cost of the iterative-perturbation scheme is the total number of iterations needed before the successive iterations converge to a reasonably accurate solution. Such statistics will be collected later for several numerical tests. In general, we find that no more than 10 iterations are required for static problems, while only one iteration is sufficient per time step for kinetic simulations.

4. Elastic solution in films with stress free surfaces and substrate constraints

Next, we show how to recast an elastic problem in thin films with stress-free surfaces and substrate constraints into the general framework of inhomogeneous elasticity systems introduced in Section 2. As schematically depicted in Fig. 1, we insert a gas layer on top of the film to make up a 3D bulk system on a cubic domain. The original curvy film surface becomes a diffuse interface between the solid and gas phases in the new system and thus does not require any special treatment in terms of the mesh alignment as in, for example, the finite element method. If we apply periodic boundary conditions to the new substrate–film–gas system, the iterative-perturbation scheme can be implemented on a regular mesh with the Fourier-spectral method. As in Section 2, the eigenstrain and the elastic modulus tensors are defined as

$$\varepsilon^0_{ij}(\boldsymbol{x}) = \begin{cases} \varepsilon^{\mathrm{def}}_{ij}(\boldsymbol{x}) & \text{in the gas phase,} \\ \varepsilon^{c}_{ij}(\boldsymbol{x}) + \varepsilon^{\mathrm{def}}_{ij}(\boldsymbol{x}) & \text{in film and substrate} \end{cases}$$

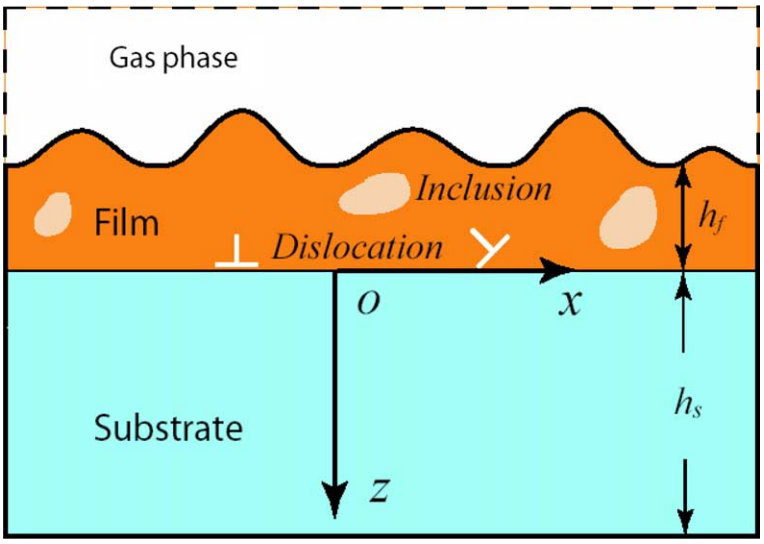

Fig. 1. Schematic view of an elastically inhomogeneous system.

and

$$\lambda_{ijkl}(\boldsymbol{x}) = \begin{cases} 0.0 & \text{in the gas phase,} \\ \lambda^0_{ijkl} + \lambda'_{ijkl}\delta c(\boldsymbol{x}) & \text{in film and substrate,} \end{cases}$$

where $\varepsilon^{\text{def}}_{ij}(\boldsymbol{x})$ is the eigenstrain associated with the distribution of defects such as real dislocations in the solid and image dislocations in the gas phase. With these coefficients, the elasticity system to be solved remains as (2.5).

Since the elastic constant is zero in the gas phase, all stress components are zero there as well. Assuming the continuity of stress at the interface between the gas and solid phases, the elastic solution thus obtained must satisfy the desired stress-free boundary conditions at the film surface ($x_3 = z = -h_f$), and the bottom of the substrate ($x_3 = z = h_s$). Later, we will provide rigorous justification for this heuristic. Without loss of generality, we assume in our analysis that both the film and the substrate are elastically homogeneous (so the inhomogeneity refers to the film–gas transition). Also in the analysis, we assume that the film surface is flat. The iterative-perturbation scheme is not limited to problems with flat film surfaces, and in fact it has been successfully employed to simulate the formation of quantum dots where the surface is rough [17].

5. Mathematical analysis

In this section, we present rigorous analysis on the formulation of the inhomogeneous elasticity problem and on the iterative-perturbation scheme used to solve the system numerically. In particular, we direct our attention to the following three key issues: (1) what is the effect of introducing a degenerate gas layer on the well-posedness of the new system? (2) In what sense is the new substrate–film–gas system an approximation to the original system consisting of the substrate and film layers only? (3) Can we guarantee the convergence of the iterative-perturbation scheme in the presence of the strong elastic inhomogeneity between the film and gas?

For a clear illustration of the main ideas, we study a simplified model equation that still captures the essential features of (2.5) needed to address the above questions. The simplified 3D model equation defined on $[0, 1]^3$ reads

$$\frac{\partial}{\partial x_j}\left[\lambda_{ijkl}a_\varepsilon(x_3)\frac{\partial u_k}{\partial x_l}\right] = \frac{\partial}{\partial x_j}\left[\lambda_{ijkl}a_\varepsilon(x_3)b_\varepsilon^{kl}(\boldsymbol{x})\right] \tag{5.1}$$

with periodic boundary conditions. Here, λ_{ijkl} is a constant elasticity tensor which is symmetric positive definite, and the elastic inhomogeneity between the solid and gas phases is characterized by the scalar function $a_\varepsilon(x_3)$ which depends only on the x_3 direction. The function $a_\varepsilon(x_3)$ is a mollified version of the characteristic function $a(x_3)$ of the substrate and film layers, i.e., $a(x_3) = 1$ for $0 < x_3 < h_0$ where h_0 is the height of the top of the film, and $a(x_3) = 0$ elsewhere. The small parameter ε denotes the thickness of the diffuse interface between the gas layer and the film layer, and it goes to zero in the sharp interface limit. We will see in the later discussion that the details of the mollification process are not important so long as we have the desired bounds, smoothness and convergence properties. Similarly, $b_\varepsilon^{kl}(x)$ is the mollified version of the applied strain $b^{kl}(\boldsymbol{x})$ corresponding to the original substrate and film system, which vanishes in the gas layer ($h_0 < x_3 < 1$). The model equation makes the simplifying assumption of the film top being flat and the elasticity tensor being homogeneous within the substrate and film, but still preserves the strong elastic inhomogeneity caused by the gas layer, which is the major concern of our formulation of the elasticity system.

First of all, the existence of solution to (5.1) can be easily established by considering the associated variational problem [25] with the standard elastic energy,

$$\frac{1}{2}\int \lambda_{ijkl}a_\varepsilon(x_3)\left[\frac{\partial u_i}{\partial x_j} - b_\varepsilon^{ij}\right]\left[\frac{\partial u_k}{\partial x_l} - b_\varepsilon^{kl}\right]\mathrm{d}x$$

over the space $H_p^1((0,1)^3)$ of functions in the Sobolev space $H^1((0,1)^3)$ [26] that satisfies the periodic boundary condition. However, a peculiar consequence of the degeneracy in the gas layer is that the solution is not unique there. Fortunately, this little "inconvenience" can be safely ignored since we are only interested in the solution to (5.1) in the substrate and film layers. We note that multiplying (5.1) with zero right-hand side by u_i and integrating by parts immediately lead to the uniqueness (up to a constant) of the solution where the elasticity tensor is non-degenerate. Therefore, we have shown that *the solution to the (partially degenerate) elasticity equations (5.1) exists and is unique in the substrate and film layers.*

To reveal the relation between the diffuse-interface description of the substrate, film and gas system and the original substrate and film system, we next study the sharp-interface limit of (5.1) in its weak formulation as the small parameter ε approaches zero. To derive the limiting equation, we multiply (5.1) by an arbitrary smooth test function v_i, compactly supported in $(0, 1) \times (0, 1) \times (0, h_0)$, and perform integration by parts. We get the weak formulation of the equation with mollified coefficients,

$$\int_0^{h_0}\int_0^1\int_0^1 \lambda_{ijkl}a_\varepsilon(x_3)\frac{\partial u_k^\varepsilon}{\partial x_l}\frac{\partial v_i}{\partial x_j}\,\mathrm{d}x_1\,\mathrm{d}x_2\,\mathrm{d}x_3 = \int_0^{h_0}\int_0^1\int_0^1 \lambda_{ijkl}a_\varepsilon(x_3)b_\varepsilon^{kl}(x)\frac{\partial v_i}{\partial x_j}\,\mathrm{d}x_1\,\mathrm{d}x_2\,\mathrm{d}x_3, \tag{5.2}$$

where u^ε denotes a solution in $H_p^1((0,1)^3)$ to (5.1) for a given ε. To pass to the limit, we need the following uniform bound on u^ε,

$$\int_0^{h_0}\int_0^1\int_0^1 \sum_{k,l}\left|\frac{\partial u_k^\varepsilon}{\partial x_l}\right|^2 \mathrm{d}x_1\,\mathrm{d}x_2\,\mathrm{d}x_3 < M$$

which can be easily proven from the positive-definiteness of the elasticity tensor. Now, denoting the weak limit (up to a constant) of u^ε by u^0 (its uniqueness can be easily seen from the limiting equation and the boundary condition derived later), we may let ε go to zero in (5.2) and obtain

$$\int_0^{h_0}\int_0^1\int_0^1 \lambda_{ijkl}\frac{\partial u_k^0}{\partial x_l}\frac{\partial v_i}{\partial x_j}\,dx_1\,dx_2\,dx_3 = \int_0^{h_0}\int_0^1\int_0^1 \lambda_{ijkl}b^{kl}(\boldsymbol{x})\frac{\partial v_i}{\partial x_j}\,dx_1\,dx_2\,dx_3 \tag{5.3}$$

which is exactly the weak formulation of the substrate and film system,

$$\frac{\partial}{\partial x_j}\left[\lambda_{ijkl}\frac{\partial u_k}{\partial x_l}\right] = \frac{\partial}{\partial x_j}\left[\lambda_{ijkl}b^{kl}(\boldsymbol{x})\right] \tag{5.4}$$

defined on $(0,1)\times(0,1)\times(0,h_0)$.

But what are the boundary conditions for Eq. (5.4) as a result of passing the solutions of (5.1) to the weak limit? To derive the boundary conditions, we choose a general smooth periodic test function v, not necessarily compactly supported in $(0,1)\times(0,1)\times(0,h_0)$. Proceeding similarly as above, we arrive at

$$\int_0^1\int_0^1\int_0^1 \lambda_{ijkl}a_\varepsilon(x_3)\frac{\partial u_k^\varepsilon}{\partial x_l}\frac{\partial v_i}{\partial x_j}\,dx_1\,dx_2\,dx_3 = \int_0^1\int_0^1\int_0^1 \lambda_{ijkl}a_\varepsilon(x_3)b_\varepsilon^{kl}(\boldsymbol{x})\frac{\partial v_i}{\partial x_j}\,dx_1\,dx_2\,dx_3. \tag{5.5}$$

The limit of the right-hand side as $\varepsilon\to 0$ is obviously $\int_0^{h_0}\int_0^1\int_0^1 \lambda_{ijkl}b^{kl}(\boldsymbol{x})\frac{\partial v_i}{\partial x_j}\,dx_1\,dx_2\,dx_3$. To analyze the left-hand side, we split it into two integrals over the domain $(0,1)\times(0,1)\times(0,h_0)$ and $(0,1)\times(0,1)\times(h_0,1)$. As before, the first integral tends to $\int_0^{h_0}\int_0^1\int_0^1 \lambda_{ijkl}\frac{\partial u_k^0}{\partial x_l}\frac{\partial v_i}{\partial x_j}\,dx_1\,dx_2\,dx_3$. Let X_{ijkl} be the square root tensor of λ_{ijkl}, i.e. $\lambda_{ijkl} = X_{ijmn}X_{mnkl}$. The Cauchy–Schwarz inequality applied to the second integral gives

$$\begin{aligned}\left|\int_{h_0}^1\int_0^1\int_0^1 \lambda_{ijkl}a_\varepsilon(x_3)\frac{\partial u_k^\varepsilon}{\partial x_l}\frac{\partial v_i}{\partial x_j}\,dx_1\,dx_2\,dx_3\right| &\leqslant \int_{h_0}^1\int_0^1\int_0^1 \left|X_{ijmn}\sqrt{a_\varepsilon}\frac{\partial v_i}{\partial x_j}\right|\left|X_{mnkl}\sqrt{a_\varepsilon}\frac{\partial u_k^\varepsilon}{\partial x_l}\right|dx_1\,dx_2\,dx_3\\ &\leqslant \left[\int_{h_0}^1\int_0^1\int_0^1 \lambda_{ijkl}a_\varepsilon(x_3)\frac{\partial v_k}{\partial x_l}\frac{\partial v_i}{\partial x_j}\,dx_1\,dx_2\,dx_3\right]^{\frac{1}{2}}\\ &\quad\times\left[\int_{h_0}^1\int_0^1\int_0^1 \lambda_{ijkl}a_\varepsilon(x_3)\frac{\partial u_k^\varepsilon}{\partial x_l}\frac{\partial u_i^\varepsilon}{\partial x_j}\,dx_1\,dx_2\,dx_3\right]^{\frac{1}{2}}.\end{aligned}$$

Due to the fact that $a_\varepsilon(x_3)$ approaches the step function $a(x_3)$ which vanishes where $r_3 > h_0$, the first factor in the product on the right-hand side of the above equation goes to zero as $\varepsilon\to 0$. On the other hand, we can show, by multiplying (5.1) by u_i^ε and then applying integration by parts and the Cauchy–Schwarz inequality as before, that the second factor is uniformly bounded independent of ε. Therefore, we have that

$$\int_{h_0}^1\int_0^1\int_0^1 \lambda_{ijkl}a_\varepsilon(x_3)\frac{\partial u_k^\varepsilon}{\partial x_l}\frac{\partial v_i}{\partial x_j}\,dx_1\,dx_2\,dx_3 \to 0 \quad \text{as } \varepsilon\to 0.$$

Now, passing to the limit in (5.5), we recover the same equation (5.3), except that in the present case the test function v_i does not vanish in general at the boundaries of the substrate and film system at $x_3 = 0, h_0$. Thus in addition to the PDE (5.4), Eq. (5.3) also gives rise to the natural boundary condition,

$$\lambda_{ijkl}\left(\frac{\partial u_k}{\partial x_l} - b^{kl}\right)n_j = 0 \quad \text{for } i = 1,2,3,$$

where n_j is the jth component of the normal vector to the boundary. It states that the normal stress component vanishes at the boundaries of the substrate and film system. In short, we have shown that, *in the sharp interface (between the film and gas) limit, the proposed substrate, film and gas formulation converges to the original substrate and film system (5.4) with the stress-free boundary condition at the top of the film and the bottom of the substrate*. This is consistent with the heuristic argument in Section 3.

To address the third question raised in the beginning of this section, we study the convergence of the iterative-perturbation scheme used to solve the substrate, film and gas system. Since the inhomogeneous part of the elasticity tensor is represented by $a_\varepsilon(x_3) - 1$, the iterative-perturbation scheme applied to the 3D model equation reads

$$\frac{\partial}{\partial x_j}\left[\lambda_{ijkl}\frac{\partial}{\partial x_l}u_k^{(n)}\right] = -\frac{\partial}{\partial x_j}\left[\lambda_{ijkl}(a_\varepsilon(x_3)-1)\frac{\partial}{\partial x_l}u_k^{(n-1)}\right] + \frac{\partial}{\partial x_j}\left[\lambda_{ijkl}a_\varepsilon(x_3)b_\varepsilon^{kl}\right]. \tag{5.6}$$

We assume u_k^∞ is a solution to (5.1), and set $\tilde{u}_k^{(n)} = u_k^{(n)} - u_k^\infty$. Then, $\tilde{u}_k^{(n)}$ satisfies the recursive relation

$$\frac{\partial}{\partial x_j}\left[\lambda_{ijkl}\frac{\partial}{\partial x_l}\tilde{u}_k^{(n)}\right] = -\frac{\partial}{\partial x_j}\left[\lambda_{ijkl}(a_\varepsilon(x_3)-1)\frac{\partial}{\partial x_l}\tilde{u}_k^{(n-1)}\right]. \tag{5.7}$$

Multiplying Eq. (5.7) by $\tilde{u}_k^{(n)}$, integrating it by parts, applying the Cauchy–Schwarz inequality as before, and using the fact that $0 \leqslant a_\varepsilon \leqslant 1$, one can show that $\int_0^1\int_0^1\int_0^1 \lambda_{ijkl}\frac{\partial\tilde{u}_k^{(n)}}{\partial x_l}\frac{\partial\tilde{u}_i^{(n)}}{\partial x_j}\,dx_1\,dx_2\,dx_3$ is uniformly bounded, and so is $\left\|\frac{\partial\tilde{u}_k^{(n)}}{\partial r_l}\right\|_{L^2}$ due to the positive definiteness of the elasticity tensor. Thus, assuming that $\int_0^1\int_0^1\int_0^1 \tilde{u}_k^{(n)}\,dx_1\,dx_2\,dx_3 = 0$ for all n, there exists a subsequence of $\{\tilde{u}_k^{(n)}\}$ that converges weakly in H_p^1 to a weak solution of (5.1) with zero right-hand side. Inside the substrate and film, the weak solution to (5.1) with zero right-hand side is unique and is zero. Thus, the weak limit of the corresponding subsequence of $\{\tilde{u}_k^{(n)}\}$ can only be a modification of u_k^∞ in the gas. In this sense, the weak limit is independent of any particularly chosen subsequence, and thus the whole sequence $\{\tilde{u}_k^{(n)}\}$ converges weakly in H_p^1. So we have seen that *the iterative-perturbation scheme at least converges weakly in H_p^1 to the solution of the elasticity equations*. We make two additional comments. First, if the inhomogeneity parameter $a_\varepsilon(x_3)$ does not completely vanish in the gas layer, the above argument actually gives the strong convergence in H_p^1 (i.e, convergence in norm) with a geometric convergence rate. Second, in the general case, as long as the inhomogeneous part of the elasticity tensor which we split to the right-hand side of the iterative-perturbation scheme can be majorized by the remaining tensor on the left-hand side, the above argument still applies.

In summary, the above analysis has established for the model Eqs. (5.1) that the iterative-perturbation scheme (5.6) converges to an elastic solution to the diffuse-interface description of the substrate–film–gas system, and in the sharp interface limit, this solution converges to that of the original substrate-film system (5.4) with stress-free boundary conditions. We have assumed that each step of the iterative-perturbation scheme can be solved accurately with the Fourier-spectral method, and thus have not included the numerical errors in our analysis. Although the analysis assumes periodic boundary conditions, the well-posedness and the convergence arguments are in fact independent of the particular boundary conditions. Moreover, with some modification to details, we believe the analysis can be generalized to other elasticity systems with degeneracy, such as films with curvy surfaces, voids, cracks, etc. Numerical tests on systems with voids to be presented in the next section reinforce that the proposed approach works on general elasticity systems with degeneracy.

6. Numerical tests

We test the proposed method on two static elasticity problems and a kinetic simulation of microstructure evolution under the influence of elastic inhomogeneity. The two static problems can be solved analytically and the numerical solutions are compared against the analytical ones to validate the convergence and efficiency of the proposed scheme. The kinetic problem illustrates some interesting effects of elastic inhomogeneity on thin film morphologies.

6.1. Static problems

We choose two elastic boundary value problems with analytical solutions: the uni-axial tensile of an elastic body with a circular void at the center, and the edge dislocation in a half-infinite elastic body [19,27]. First we consider an elastic body with a central void under applied stresses $\sigma_{zz}^0/G = 0.1$ and $\sigma_{xx}^0/G = 0$

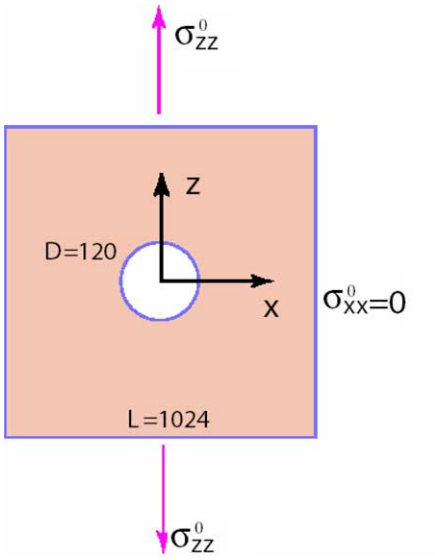

Fig. 2. Plane strain problem: uni-axial tensile of an elastic body with a circular void.

where G is the shear modulus. The simulation cell is 1024×1024 as shown in Fig. 2. The diameter of the central void is $D = 120$. The dimensionless elastic constants are $C_{11}/G = 3$, $C_{12}/G = 1$ and $C_{44}/G = 1$ while they are zero in the void. Distributions of stress components σ_{xx}, σ_{zz} and σ_{xx} along x and z axes, which are obtained by the iteration method, are plotted by the dot symbols in Fig. 3(a) and (b) where the analytical solutions are plotted with solid lines. Comparison of stress fields in x–z plane is presented in Fig. 4. Considering that the analytical solution is for the sharp interface model while our numerical solution is for the diffuse-interface description, the results demonstrate that the iteration scheme is able to provide excellent solutions for strongly inhomogeneous elasticity system with voids. Furthermore, the iterative-perturbation scheme converges in only 6–8 steps.

Next let us examine the convergence of the iteration method by numerically solving the dislocation elastic solution which has a strong stress concentration. The simulation cell is 512×256 as shown in Fig. 5, where $h = 40$ and $l = 1$. The elastic constants used are the same as that in the first example. The dislocation below the surface and its image dislocation in the gas phase form a dislocation loop. The non-zero eigenstrain associated with such a dislocation loop is

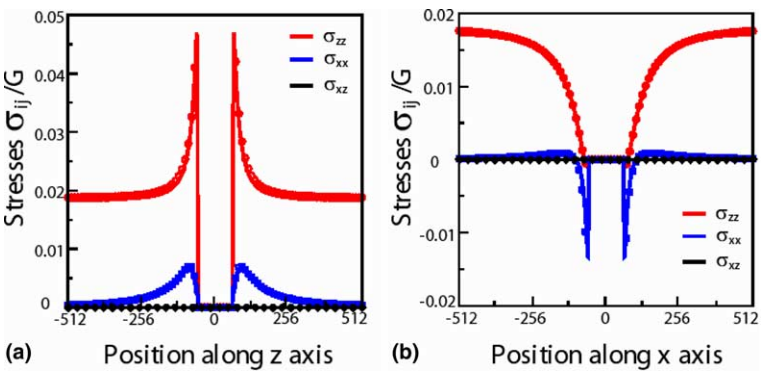

Fig. 3. Comparison of stress distributions along x- and z-axes: symbol for numerical solution and solid line for analytical solution.

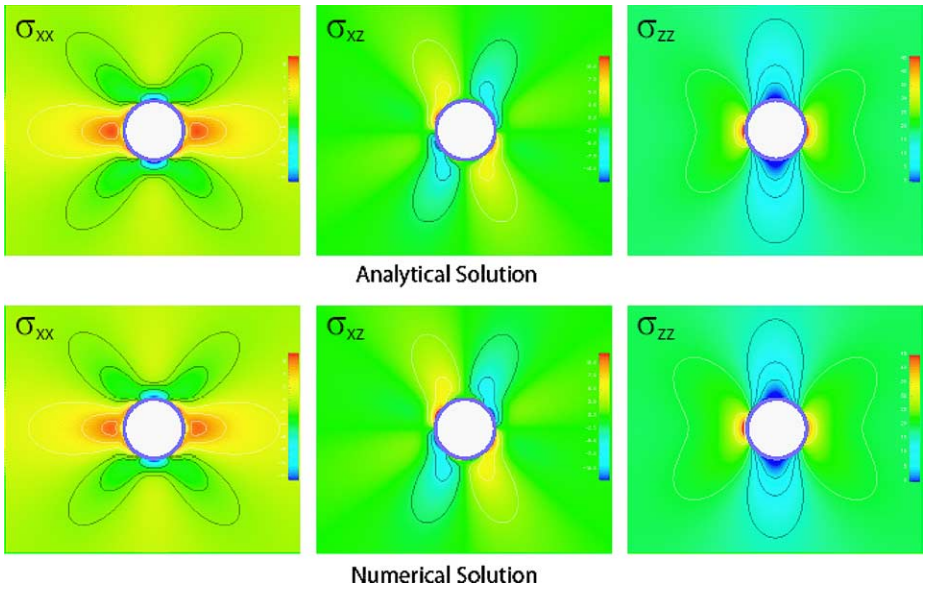

Fig. 4. Comparison of the stress field obtained by analytical and numerical solutions around the void under uni-axial tensile stress.

$$\varepsilon_{11}^{\mathrm{def}}(\boldsymbol{x}) = b/d_0\delta(\boldsymbol{x} - \boldsymbol{x}_0),$$

where b is the magnitude of the Burgers vector of the dislocation, d_0 is the grid spacing. $\boldsymbol{x}_0$ is the point within the dislocation loop. Distributions of stress components $\sigma_{xx}(z)$ and $\sigma_{zz}(z)$ along A–A line shown in Fig. 5 are plotted in Figs. 6 and 7 for different iteration numbers. The analytical solutions are also included for a comparison. It is found that the numerical solution with only 8 iterations agrees very well with the analytical solution. In fact, the number of iterations can be further reduced in time-dependent problems of

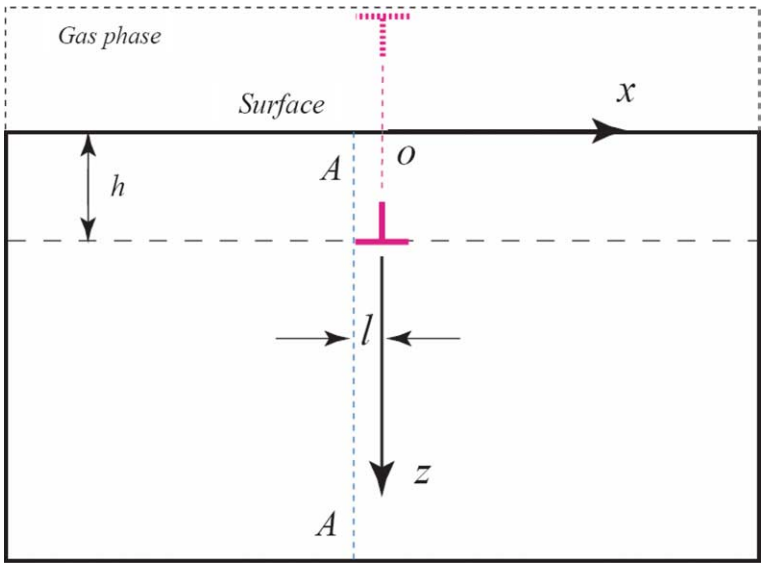

Fig. 5. The image dislocation in the gas phase and the real dislocation below the surface form a dislocation loop.

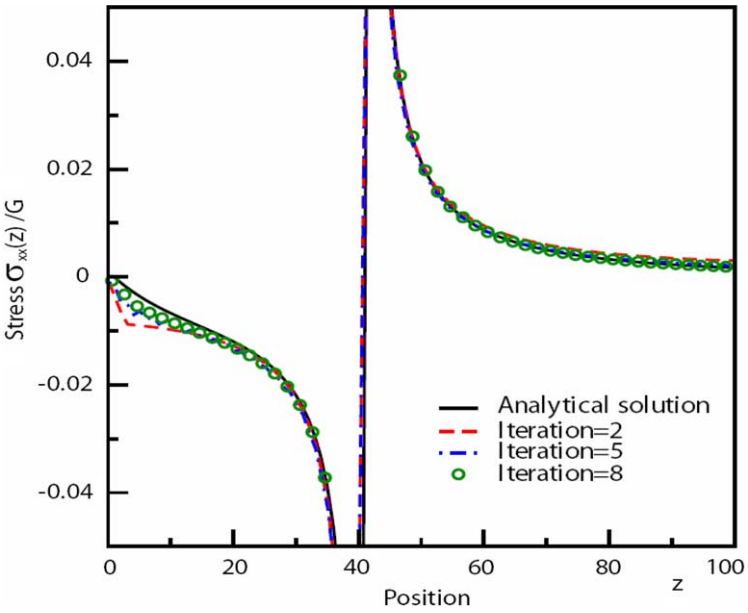

Fig. 6. Stress component: $\sigma_{xx}(z)/G$ along A–A line shown in Fig. 5.

microstructure evolution. In such problems, if the elastic solution at time t is used as the zeroth iterate for the iterative-perturbation scheme at time $t + \Delta t$, often only one iteration is sufficient to maintain the convergence of the elastic solution. Thus, the proposed scheme applied to this strongly inhomogeneous system is as efficient as the case when it is applied to homogeneous systems!

6.2. Kinetic simulation in thin films

6.2.1. Coupling with the phase-field simulation

The main goal of solving the elasticity equations is to obtain the elasticity energy needed in the phase-field simulation of microstructure evolution. In this section, we apply the iterative-perturbation scheme coupled with the semi-implicit Fourier-spectral method for the phase-field simulation of the effect of the elastic inhomogeneity on the occurrence of various morphological patterns in thin films. For simplicity, we assume the film is a binary solid solution, which is unstable with respect to phase separation at the temperature of interest. One field variable $c(\boldsymbol{x}, t)$ representing the mole or atom fraction at position $\boldsymbol{x}$ and time t, is needed to describe the composition evolution or the morphological evolution of the separated phases. Then, the total free energy of the system includes three contributions: bulk chemical free energy, interfacial energy and elastic energy,

$$F = \int_v \left[f(c(\boldsymbol{x},t),T) + \frac{\kappa^2}{2}(\nabla c(\boldsymbol{x},t))^2 + \frac{1}{2}\lambda_{ijkl}(\boldsymbol{x},t)\varepsilon_{elij}(\boldsymbol{x},t)\varepsilon_{elkl}(\boldsymbol{x},t) \right] \mathrm{d}^3x, \tag{6.1}$$

where $f(c, T)$ is the chemical free energy density of the solid solution, κ is the gradient energy coefficient which is determined by the interfacial energy and thickness. The third term in (6.1) is the elastic energy density given by

$$e_{\mathrm{el}} = \frac{1}{2}\lambda_{ijkl}\varepsilon_{ij}^{\mathrm{el}}\varepsilon_{kl}^{\mathrm{el}} = \frac{1}{2}[\lambda_{ijkl}^{0} + \lambda'_{ijkl}\delta c(\boldsymbol{x})][\bar{\varepsilon}_{ij} + \delta\varepsilon_{ij}(\boldsymbol{x}) - \varepsilon_{ij}^{c}(\boldsymbol{x}) - \varepsilon_{ij}^{\mathrm{def}}(\boldsymbol{x})][\bar{\varepsilon}_{ij} + \delta\varepsilon_{kl}(\boldsymbol{x}) - \varepsilon_{kl}^{c}(\boldsymbol{x}) - \varepsilon_{kl}^{\mathrm{def}}(\boldsymbol{x})]. \tag{6.2}$$

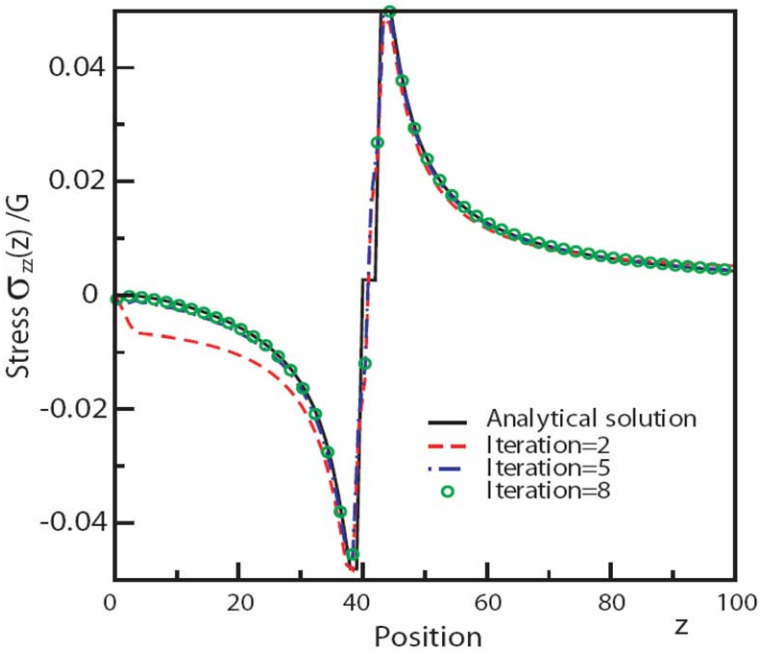

Fig. 7. Stress Component: σ_{zz} $(z)/G$ along A–A line shown in Fig. 5.

In Eq. (6.2), $\delta\varepsilon_{kl}(\boldsymbol{x})$ is given by

$$\delta\varepsilon_{ij}(\boldsymbol{x}) = \frac{1}{(2\pi)^3}\int \frac{\mathrm{i}}{2}\left[v_i(\boldsymbol{g})g_j + v_j(\boldsymbol{g})g_i\right]\mathrm{e}^{\mathrm{i}\boldsymbol{g}\cdot\boldsymbol{x}}\,\mathrm{d}^3\boldsymbol{g},$$

where $v_i(\boldsymbol{g})$ is the ith component of the solution to the elasticity equations in the Fourier space. The corresponding elastic stress is given by Eq. (2.1). The homogeneous strain in Eqs. (2.3) and (2.5) is determined by the boundary conditions. If the boundary is clamped so that the system is not allowed to have any homogeneous deformation, the homogeneous strain $\bar{\varepsilon}_{ij}$ is equal to zero. Similarly, if the system is subject to an initial applied strain, ε^a_{ij}, then the boundary is held fixed, $\bar{\varepsilon}_{ij} = \varepsilon^a_{ij}$. On the other hand, if the system is stress-free, i.e., the system is allowed to deform so that the average stress in the system is zero, the homogeneous strain is obtained by minimizing the total elastic energy with respect to the homogeneous strain.

Since the composition is a conserved field variable, the kinetic equation of the composition field is described by the Cahn–Hilliard type diffusion equation [28] given by

$$\frac{\partial c(\boldsymbol{x},t)}{\partial t} = \nabla\cdot M\nabla\frac{\delta E}{\delta c(\boldsymbol{x},t)} + \xi(\boldsymbol{x},t) = \nabla\cdot M\nabla\left[\frac{\mathrm{d}f(c(\boldsymbol{x},t),T)}{\mathrm{d}c(\boldsymbol{x},t)} - \kappa^2\nabla^2 c(\boldsymbol{x},t) + \mu_{\mathrm{el}}\right] + \xi(\boldsymbol{x},t), \tag{6.3}$$

where $\xi(\boldsymbol{x}, t)$ is a noise term representing the composition fluctuation which is only applied at the initial moment of the simulation, and M is the chemical mobility. If we assume that the atomic mobility of species 1 and 2 are equal, the mobility M is given by

$$M = \frac{Dc(\boldsymbol{x},t)(1-c(\boldsymbol{x},t))}{k_{\mathrm{B}}T},$$

where D is the chemical diffusion coefficient, k_{B} is the Boltzmann constant and T is the temperature. The mobility is further simplified by assuming that the factor $c(\boldsymbol{x}, t)(1 - c(\boldsymbol{x}, t))$ is a constant given by $c_0(1 - c_0)$ where c_0 is the overall composition.

The chemical free energy density of the solid solution is expressed as $f(c(\boldsymbol{x}, t),T) = -(c(\boldsymbol{x}, t) - 0.5)^2 + 2.5(c(\boldsymbol{x}, t) - 0.5)^4$, which determines the equilibrium compositions at c = 0.053 or 0.947. In (6.3), μ_{el} is the elastic potential due to the coherency strain, which is the derivative of the elastic energy density with respect to the composition.

In the present work, we ignore the morphological instabilities on the film surface, and assume the composition flux at the surface of the film and interface between the film and the substrate are zero. Therefore, the temporal evolution of the composition field is obtained by solving Eq. (6.3) together with the initial conditions and the following boundary conditions:

$$\left.\frac{\partial c(\boldsymbol{x},t)}{\partial z}\right|_{z=-h_f} = 0 \quad \text{and} \quad \left.\frac{\partial c(\boldsymbol{x},t)}{\partial z}\right|_{z=0} = 0.$$

To numerically solve this evolution equation, a Fourier-spectral method is used in x and y directions [29,30]. Since the zero-flux boundary conditions at film surface and film/substrate interface cannot be satisfied by a Fourier expansion, a second-order finite difference method is used in the z-direction and also solved with FFT. (Note that this complication only arises for the Cahn–Hilliard equation, not for the elasticity equations.) The semi-implicit scheme is used for the time integration for simplicity, although in principle higher-order time integration schemes are also available [31].

6.2.2. Simulation results

The effect of elastic inhomogeneity on microstructures is studied in a film which undergoes a phase separation. In the simulation, $64 \times 64 \times 64$ discrete grid points are used. The thickness of the substrate is $36d^*$, and the film thickness is $4d^*$. The dimensionless grid spacing is chosen to be $d^* = \Delta x_1/d_0 = \Delta x_2/d_0 = \Delta x_3/d_0 = 1.0$ and the dimensionless time step $\Delta t^* = D\Delta t c_0(1 - c_0)/d_0^2 = 0.05$. The interfacial energy is assumed to be isotropic, and the dimensionless gradient energy coefficient, $\alpha^* = \alpha/(k_B T d_0^2)$, is taken to be 0.5. The overall composition used is $c_0 = 0.67$ which is inside the spinodal decomposition region. According to the level rule, the equilibrium volume fraction of the solute rich phase (γ phase) is about 67%, and 33% for the solvent rich phase (β phase). In order to examine the effect of the shear modulus on the microstructure evolution, we assume that the bulk moduli of two phases are the same, and vary the shear moduli of two phases. Elastic constants for the three cases are listed in Table 1. In Case 1 the γ phase has larger shear modulus than the β phase while the γ phase has smaller shear modulus than the β phase in Case 3. In Case 2 the system is elastically homogeneous.

The simulations start with a small composition perturbation. Fig. 8 presents the temporal evolution of microstructures. The blue domain denotes the β phase while the red domain for γ phase. It is observed that for three different cases the phase separation all took place first near the free surface. The simulations demonstrate that the morphologies strongly depend on the difference in shear modulus as well as the volume fractions of two phases. In Case 1 with a combination of a lower volume fraction of the soft phase, the β phase which has smaller shear modulus, and a higher volume fraction of the hard phase, the phase separation favors the formation of a network of two phases. However, in Case 3 where there is a combination of a higher volume fraction of soft phase and a lower volume fraction of hard phase, it is found that the soft

Table 1
Elastic constants (GPa) for three model systems

Case	γ phase			β phase		
	C_{11}	C_{12}	C_{44}	C_{11}	C_{12}	C_{44}
Case 1	232.0	153.0	117.0	197.0	188.0	13.3
Case 2	220.3	164.7	82.3	220.3	164.7	82.3
Case 3	208.5	176.5	47.5	243.5	141.5	151.2

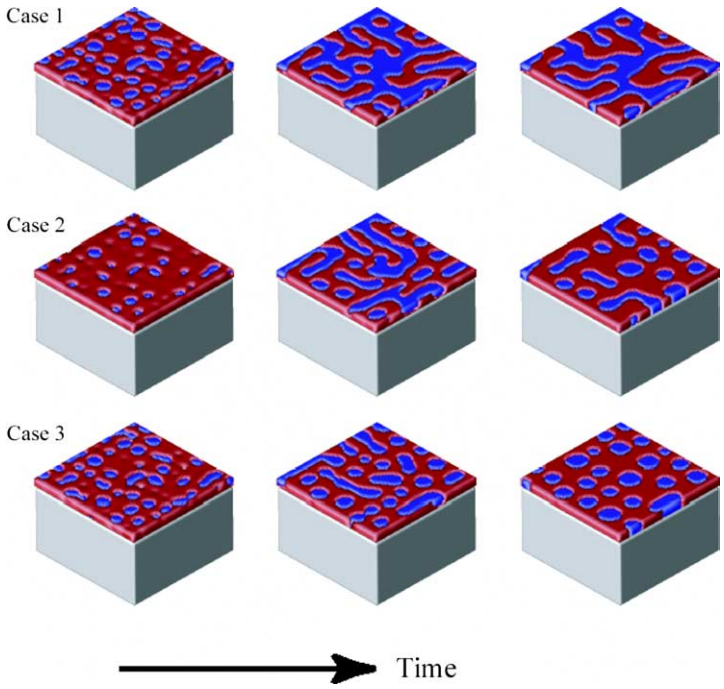

Fig. 8. Effect of inhomogeneous shear modulus on microstructure evolution in films.

phase forms a connected domain while the harder phase forms isolated particles. For the elastically homogeneous case in Case 2, the lower volume fraction phase still forms isolated particles, but the sizes of particles are larger than that in Cases 3. This implies that the elastic inhomogeneity refines the particle size. More systematic and quantitative studies on the effect of elastic inhomogeneity and thin film thickness on morphologies of phase separation will be reported in our upcoming papers. Finally, we note that only one iteration of the iterative-perturbation scheme is needed at each time step of our simulation.

7. Conclusion

We presented a simple and efficient approach to treat elasticity systems with strong inhomogeneity. We have also provided rigorous justification for our formulation of the diffuse-interface model and the numerical scheme. Several numerical tests have been performed to confirm the validity and the efficiency of the method. The focus of the current paper is on the method and analysis. More challenging simulation studies using the proposed method that may involve evolving film surfaces, voids or cracks will be reported in our future work.

Acknowledgement

The authors are grateful for the financial support from NSF under the Grant Nos. DMS-0409297, DMR-0122638 and DMR-0205232, and ALCOA.

References

[1] L.Q. Chen, Phase-field models for microstructure evolution, Ann. Rev. Mater. Res. 32 (2002) 113.
[2] A.G. Khachaturyan, Theory of Structural Transformations in Solids, Wiley, New York, 1983.
[3] A. Onuki, H. Nishimori, Anomalously slow domain growth due to a modulus inhomogeneity in phase-separation alloys, Phys. Rev. B 43 (1991) 13649.
[4] A. Onuki, Ginzburg–Landau approach to elastic effects in the phase-separation of solids, J. Phys. Soc. Jpn. 58 (1989) 3065.
[5] C. Sagui, A.M. Somoza, R. Desai, Spinodal decomposition in an order–disorder phase-transition with elastic fields, Phys. Rev. E 50 (1994) 4865.
[6] S.Y. Hu, L.Q. Chen, A phase-field model for evolving microstructures with strong elastic inhomogeneity, Acta Mater. 49 (2001) 1879.
[7] P.H. Leo, J.S. Lowengrub, H.J. Hou, A diffuse interface model for microstructure evolution in elastically stressed solids, Acta Mater. 61 (1998) 2113.
[8] J. Zhu, L.Q. Chen, J. Shen, Computer simulation of morphological evolution during phase separation and coarsening with strong inhomogeneous elasticity, Model. Simulat. Mater. Sci. Eng. 9 (2001) 499.
[9] D.N. Bhate, A. Kumar, A.F. Bower, Diffuse interface model for electromigration and stress voiding, J. Appl. Phys. 87 (2000) 1712.
[10] Y.U. Wang, Y.M. Jin, A.G. Khachaturyan, Three-dimensional phase field microelasticity theory and modeling of multiple cracks and voids, Appl. Phys. Lett. 78 (2001) 3071.
[11] Y.U. Wang, J.M. Jin, A.M. Cuitino, A.G. Khachaturyan, Nanoscale phase field microelasticity theory of dislocations: model and 3D simulations, Acta Mater. 49 (2001) 1847.
[12] J.D. Eshelby, The elastic field outside an ellipsoidal inclusion, Proc. Roy Soc. A 252 (1959) 561.
[13] J.D. Eshelby, Elastic inclusions and inhomogeneities, Prog. Solid Mech. 2 (1961) 89.
[14] S.Y. Hu, L.Q. Chen, Spinodal decomposition in a film with periodically distributed interfacial dislocations, Acta Mater. 52 (2004) 3069.
[15] W. Lu, Z. Suo, Dynamics of nanoscale pattern formation of an epitaxial monolayer, J. Mech. Phys. Solids 49 (2001) 1937–1950.
[16] Y.L. Li, S.Y. Hu, Z.K. Liu, L.Q. Chen, Phase-field model of domain structures in ferroelectric thin films, Appl. Phys. Lett. 78 (2001) 3878.
[17] D.J. Seol, S.Y. Hu, Z.K. Liu, S.G. Kim, K.H. Oh, L.Q. Chen, Phase-field modeling of stress-induced surface instabilities in heteroepitaxial thin films, J. Appl. Phys., submitted for publication.
[18] T. Mura, Micromechanics of Defects in Solids, Kluwer Academic Publishers, 1982.
[19] V.L. Indenbom, J. Lothe, first ed.Elastic Strain Fields and Dislocation Mobility, vol. 31, Elsevier, North-Holland, 1992.
[20] S.Y. Hu, L.Q. Chen, Solute segregation and coherent nucleation and growth near a dislocation – a phase-field model integrating defect and phase microstructures, Acta Mater. 49 (2001) 463.
[21] Y.U. Wang, Y.M. Jin, A.M. Cuitino, A.G. Khachaturyan, Phase field microelasticity theory and modeling of multiple dislocation dynamics, Appl. Phys. Lett. 78 (2001) 2324.
[22] D. Rodney, Y. Le Bouar, A. Finel, Phase field methods and dislocations, Acta Mater. 51 (2003) 17.
[23] C. Shen, Y. Wang, Phase field model of dislocation networks, Acta Mater. 51 (2003) 2595.
[24] S.Y. Hu, Y.L. Li, Y.X. Zheng, L.Q. Chen, Effect of solutes on dislocation motion – a phase-field simulation, J. Plasticity 20 (2004) 403.
[25] K. Atkinson, W. Han, Theoretical Numerical Analysis: A Functional Analysis Framework, Springer-Verlag, 2001.
[26] R.A. Adams, Sobolev spaces, Academic Press (1975).
[27] S. Timoshenko, Theory of Elasticity, McGraw-Hill, 1951.
[28] J.W. Cahn, On spinodal decomposition, Acta Metall. 9 (1961) 795.
[29] D.J. Seol, S.Y. Hu, Y.L. Li, J. Shen, K.H. Oh, L.Q. Chen, Phase-field simulation of spinodal decomposition in elastically constrained films, Acta Mater. 51 (2003) 5173.
[30] L.Q. Chen, J. Shen, Application of semi-implicit Fourier-spectral method to phase field equations, Comput. Phys. Comm. 108 (1998) 147.
[31] Q. Du, W. Zhu, Stability analysis and applications of the exponential time differencing schemes, J. Comput. Math. 22 (2004) 200.